SIMULTANEOUS CONTROL OF UNBURNED NH_3 AND NO_X EMISSIONS FROM HIGH LOAD DUAL-FUEL AMMONIA OPERATION ON A HIGH-SPEED DIESEL ENGINE USING A CU-SCR SYSTEM

Daanish Tyrewala*, Vitaly Prikhodko, Brian Kaul, Scott Curran

Fuel Science & Engine Technologies Research Group
Oak Ridge National Laboratory, Knoxville, TN, USA
Email: tyrewalads@ornl.gov

ABSTRACT

Dual-fuel ammonia (NH_3) strategies are being investigated as a promising way to utilize NH_3 as an alternative fuel for internal combustion engines in the maritime sector. One of the remaining barriers to implementing dual-fuel NH_3 combustion strategies is understanding ways to minimize unburned NH_3 and nitrogen oxide (NO_x) emissions from these engines, both of which are elevated relative to a conventional diesel baseline. Selective catalytic reduction (SCR) systems are widely used for lean NO_x emissions controls for engines across transportation and stationary energy applications. SCR systems use a reducing agent, such as NH_3, to react with NO_x in the exhaust, converting it into nitrogen and water. Typically, NH_3 is injected into the exhaust as a urea solution. In dual-fuel NH_3 engines, where unburned NH_3 is present in the exhaust, an SCR system could be used to mitigate both NH_3 and NO_x emissions. The presented work evaluates a commercial copper-zeolite SCR and ammonia slip catalyst system, designed for on-road diesel engine applications, for controlling unburned NH_3 and NO_x emissions from a dual-fuel NH_3 combustion engine. The aftertreatment system was installed downstream of a single-cylinder four-stroke diesel engine that has been modified for dual-fuel ammonia use. The emissions were characterized by using a Fourier transform infrared spectrometer for both late- and early-injection diesel pilot strategies over three air-fuel equivalence ratios spanning from 1.6 to 1.0 at 1,200 rpm and 12.6 bar $IMEP_g$ condition (with greater than 95% ammonia energy fraction). Initial findings indicate that the SCR achieves more than 99% NO_x conversion with less than 50 ppm NH_3 slip at air-fuel equivalence ratios greater than 1.4 at the operating conditions investigated. However, these benefits are accompanied by additional N_2O emissions that are formed over the Cu-SCR.

Keywords: Ammonia, SCR, Dual-Fuel, Emissions

1. INTRODUCTION

In recent years, increasing attention has been focused on reducing emissions from the marine transportation sector. Shipping energy use—and thus emissions—is projected to increase by 50%–250% between now and 2050, subject to economic conditions [1]. Based on these estimates, the International Maritime Organization has set aggressive emissions reduction targets, including cutting CO_2-equivalent emissions from ships by 70%–80% from 2008 levels by 2040 [1,2]. Because shipping is a sector with long distance and high weight requirements, it will continue to require high-energy-density liquid fuels.

Ammonia (NH_3) serves as an alternative fuel option for maritime applications to power inland and costal marine engines, as well as freighters and tankers. It is an alkaline colorless compound with a pungent odor that serves as a hydrogen carrier. Its relatively low storage pressure (0.99 MPa vs. 69 MPa for compressed H_2) makes it economical for long-distance transportation [3]. Furthermore, its prevalent use in the agricultural sector provides readily available port infrastructure and safe handling procedures. Ammonia can be produced through electrochemical, thermochemical, and photochemical means, with the thermochemical (Haber-Bosch process) method accounting for more than 80% of total production today [4,5].

Ammonia's use as a fuel, however, comes with a unique set of challenges. The Occupational Safety and Health Administration's exposure limit for NH_3 is less than 50 ppm over a span of 8 h, which makes its toxicity a significant concern; the "immediately dangerous to life and health" threshold is 300 ppm [6]. Its low cetane number makes using it as a fuel for compression ignition (CI) applications difficult, whereas its low flame speed and high-ignition energy requirements make its

*Address all correspondence to this author

combustion challenging in a spark-ignited (SI) scenario [7]. These issues raise combustion management concerns with NH_3 because its incomplete combustion produces oxides of nitrogen such as NO_x ($NO + NO_2$) and N_2O (which has a CO_2-equivalent emissions multiplier of 273 over a span of 100 years [8]). High engine-out unburned NH_3 emissions are also an issue that requires additional attention when using NH_3 as a fuel [9, 10]. The copresence of NH_3 and NO_x in exhaust presents an opportunity to utilize existing selective catalytic reduction (SCR) and ammonia slip catalysts (ASC), which are commonly used in both stationary and mobile diesel aftertreatment applications, to simultaneously control both emissions. Traditional SCR systems use urea as a reducing agent for NO reduction [11]. However, an engine fueled directly with NH_3 provides a direct source of NH_3 for the SCR catalyst. More importantly, the presence of unburned NH_3 in the exhaust could aid in reducing NO_x over a catalyst, potentially eliminating the need for a dosing system in the exhaust. An ASC system placed downstream of the SCR can be used for minimizing NH_3 slip.

Different catalyst technologies have been identified in the literature for NO_x and N_2O abatement when using NH_3 as a fuel. For example, iron-based catalysts have been shown to simultaneously reduce NO_x and N_2O to N_2 using NH_3 [12, 13]. Voniata et al. [14] have evaluated the performance of both iron- and vanadium-based catalysts on a synthetic gas bench in simulated NH_3 engine exhaust. Their results indicated a 70%–90% reduction in CO_2-equivalent emissions compared with the emissions of conventional diesel operation for NH_3-to-NO_x ratio (ANR) less than one, whereas the cases with ANR greater than one exhibited a sevenfold CO_2-equivalent penalty, driven by high N_2O formation over the catalysts. Oh *et al.* [15] studied a conventional SCR system coupled with an ASC (no details on catalyst type were provided) for a spark-ignited ammonia/natural gas dual-fuel engine. A sweep of excess air ratio ($1 < \lambda < 1.6$) at various NH_3 energy fractions (0%–50%) resulted in under 10 ppm of NH_3 emissions downstream of their aftertreatment system. The authors also noted a small reduction in N_2O emissions downstream of the catalyst ($N_2O < 40$ ppm) but observed an unintended increase in NO_2 emissions ($NO_2 < 200$ ppm).

On a dual-fuel engine operated with diesel and NH_3, Kuta *et al.* [16] implemented a V_2O_5/SiO_2-TiO_2 SCR system. With the engine operating at mid- and high-load conditions between 40% and 60% NH_3 energy fraction, they reported NO and NO_2 conversion efficiencies greater than 80% and 60%, respectively. Only 5%–20% of residual ammonia was consumed during the NO_x reduction process, with more than 1.5% remaining untreated downstream of the SCR setup. Copper-zeolite SCR catalysts have also been studied due to their high hydrothermal stability along with the capability to adsorb/store ammonia at certain temperatures [17]. Xiang *et al.* [18] evaluated a Pt/Pd diesel oxidation catalyst (DOC) coupled with a Cu-ZSM-5 SCR on a CI engine operating on diesel and ammonia (NH_3 energy fraction: 0%–40%). The upstream placement of the DOC led to greater than 90% NH_3 conversion efficiency; however, the majority of the converted NH_3 formed N_2O. This problem worsened at higher NH_3 energy fractions as N_2O emissions increased from about 500 ppm at 10% to about 1,500 ppm under 75% load conditions. This ultimately resulted in poor NO_x conversion over the SCR as the ANR plunged below 1. The SCR's N_2O conversion efficiency was also suboptimal across the tested conditions. Similar observations were made by Sun *et al.* [19] from their 1D Cu-Zeolite SCR model coupled with a 3D diesel/NH_3 dual-fuel engine model.

In this work, a single-cylinder version of a Cummins ISB 6.7 L engine was used to perform dual-fuel NH_3 experiments at high-load and high diesel substitution (NH_3 energy fraction of about 95%) to generate a range of inlet conditions for a commercially available SCR-ASC aftertreatment system for on-road applications. The use of early- and late-pilot diesel pilot injection strategies (denoted as E-pilot and L-pilot, respectively) and a sweep of λ provide a wide range of ANR conditions for aftertreatment evaluation without a dosing system. Operation at 95% NH_3 energy fraction also allows for assessing the influence of excessively high water concentrations in the exhaust on aftertreatment performance.

2. METHODS

2.1 Engine Hardware and Fuels

The engine used for this study was a single-cylinder version of a Cummins 6.7 L ISB diesel engine. The combustion geometry was unmodified from the stock configuration. The stock diesel fuel system was retained and comprises a high-pressure common-rail direct-injection pump and a CRIN-3 eight-hole injector with a 145° included angle and a nominal diameter of 140 μm. Renewable diesel fuel sourced from Chevron Renewable Energy Group was used as the pilot fuel. The premixed chemical grade anhydrous NH_3 (Airgas) was drawn using a liquid dip tube and vaporized using a heat exchanger (heated above 55°C using hot engine-out coolant) before being measured (Emerson Micro Motion Coriolis flowmeter) and injected (two Clean Air Power DigiJet NH3ICE SP-010 injectors) 35 cm upstream of the intake port in a y-section to allow for mixing with intake air. The supply lines and flowmeter were insulated with heat tape to prevent NH_3 from condensing in the fuel system. The supply of the premixed NH_3 was interlocked

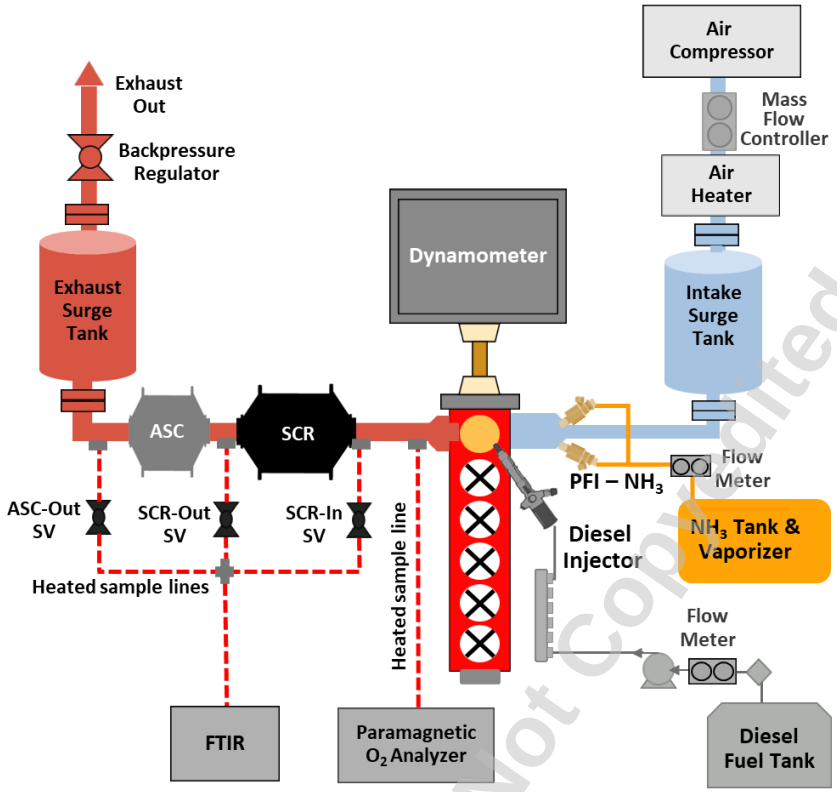

FIGURE 1: TEST SETUP SCHEMATIC.

with cell ventilation and gas monitors to ensure operator safety. The compressed air for the intake charge was conditioned using a series of air dryers and particulate filters. The temperature of the intake charge was controlled using a 6 kW heater, and the intake air mass flow rate was controlled using an Alicat Scientific mass flow controller. The engine was controlled using an open LabVIEW-based engine control system. The engine specifications are shown in Table 1, and the fuel properties in are in Table 2. Refer to Curran et al. [20] for additional details on the test setup. The engine schematic is shown in Figure 1 for reference.

TABLE 1: ENGINE SPECIFICATIONS.

Connecting Rod Length	145.4 mm
Bore × Stroke	107 × 124 mm
Displacement (1-cylinder)	1.12 L
Compression Ratio	20:1
Direct Injection System	On-engine high-pressure common-rail pump
Port Injection System	NH_3 cylinder/vaporizer

TABLE 2: FUEL PROPERTIES (1 BAR AND 20°C).

Fuel	Cetane Number	Density [kg/m^3]	LHV [MJ/kg]
Renewable Diesel	84.9	786	43.8
NH_3	~0	609	18.8

2.2 Engine Operating Conditions

The inlet conditions for the aftertreatment setup were generated from renewable diesel/NH_3 experiments conducted at an engine speed of 1,200 rpm and load of ~12.6 bar $IMEP_{net}$. Two injection strategies, E-pilot and L-pilot (shown in Figure 2), were implemented by varying the diesel start of injection (SOI) timing at a fixed global air-fuel equivalence ratio or λ. Renewable diesel was used as the pilot because its high cetane number allowed for a wider range of operability, especially for the E-pilot cases, in which combustion stability typically worsens at richer conditions. The λ for each mode was varied from about 1.6 (diesel-like) to a value of 1.0 by varying the commanded airflow (varying P_{Intake}) to the engine while maintaining an NH_3 energy fraction of ~95% (~5% diesel energy share). These sweeps were mainly motivated by potential improvements in dual-fuel NH_3 combustion performance at

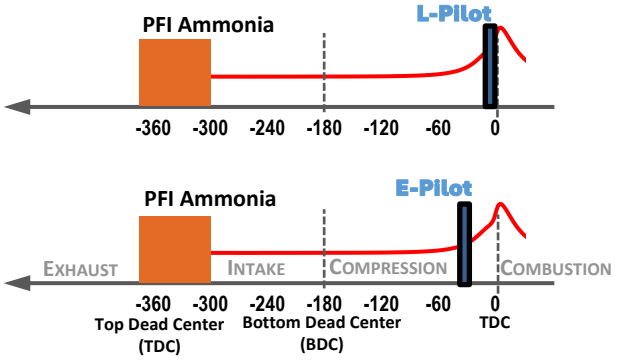

FIGURE 2: DIESEL PILOT INJECTION STRATEGIES EMPLOYED IN THE STUDY.

richer in-cylinder conditions [10]. Conventional diesel combustion (CDC) operation with a pilot + main injection at baseline manifold air pressure settings was used to provide a benchmark against which the two injection strategies could be evaluated.

Other operating condition details are as follows: intake temperature of 60°C; oil and coolant temperatures of 95°C; $P_{Intake} - P_{Exhaust}$ of ~15 kPa; and start of injection for NH_3 at 320°bTDC. The design of experiments is shown in Table 3. A total of 500 engine cycles were acquired for each point, and the low-speed data were collected simultaneously.

TABLE 3: DESIGN OF EXPERIMENTS.

Mode	λ [-]	Pilot SOI [°bTDC]
L-pilot	1.0	3/6/9/12
	1.4	
	1.6	
E-pilot	1.0	27.5/30.5/33.5
	1.4	33.5/36.5/38.5
	1.6	30.5/33.5/36.5/38.5

2.3 Catalyst Setup and Sampling Methodology

As shown in Figure 1, a commercial SCR and an ASC system were installed upstream of the exhaust surge tank. Both the catalysts, supplied by Umicore, were commercially available formulations designed specifically for on-road diesel applications. The employed SCR catalyst was a high-performance, low-temperature formulation based on copper-exchanged zeolite. It had a cell density of 400 cells per square inch (cpsi) and a washcoat loading of 200 g/L. Two monolithic SCR catalyst bricks, each measuring 14.4 cm in diameter and 12.7 cm in length, were housed in series within a stainless-steel canister. The combined volume of the SCR catalyst was 4.12 L. Positioned immediately downstream of the SCR unit was a 14.4 cm (diameter) × 5.1 cm (length) ASC catalyst. This monolith, with a total volume of 0.82 L and a cell density of 400 cpsi, utilized a precious metal Pt-based formulation with a platinum loading of 10 g/ft³.

Both the SCR and ASC were instrumented with K-type thermocouples (Omega) to measure temperatures at the inlets and outlets. Three sampling probes were installed upstream of the SCR (SCR-In), downstream of the SCR (SCR-Out), and downstream of the ASC (ASC-Out) for emissions sampling using a high-speed MKS Fourier transform infrared (FTIR) spectrometer (MKS MultiGas 2030 FTIR Gas Analyzer). The sampling locations were selected using a series of valves installed at each sampling probe. The FTIR analytical method enabled the measurement of relevant nitrogen-based (N-based) species, such as NH_3, NO, NO_2, and N_2O. The method was specifically developed to handle high levels of NH_3 in the exhaust. The sample lines were heat-traced to avoid condensation of water during sampling. A California Analytical Instruments paramagnetic O_2 analyzer was used to measure the engine-out oxygen concentration. The sampling methodology was as follows:

1. Steady-state engine operation was ensured at a λ of 1.6 and fixed pilot SOI timing using aftertreatment temperatures as an indicator.
2. The SCR-In sampling valve (SV) was first opened to collect engine-out emissions data for 500 engine cycles or ~50 seconds (SCR-Out SV and ASC-Out SV remain closed).
3. Next, the SCR-Out SV was opened and SCR-In SV closed to collect emissions data downstream of the SCR for 500 engine cycles.
4. Finally, the ASC-Out SV was opened and SCR-Out SV closed to collect emissions data downstream of the ASC for 500 engine cycles.
5. The pilot SOI timing was adjusted at the same λ, and steps 1–4 were repeated. The order of λ collection for a given injection mode was as follows: 1.6 → 1.4 → 1.0.

A leak was discovered in the SCR-Out sample line to the FTIR after data had been collected, resulting in dilution of the sample at λ = 1 conditions, where the pressure of the exhaust sample was not significantly higher than ambient pressure. A dilution ratio calculated based on the CO_2 concentrations at the SCR-In and SCR-Out locations was used to correct the FTIR emissions measurements at the SCR-Out location for the λ = 1 case.

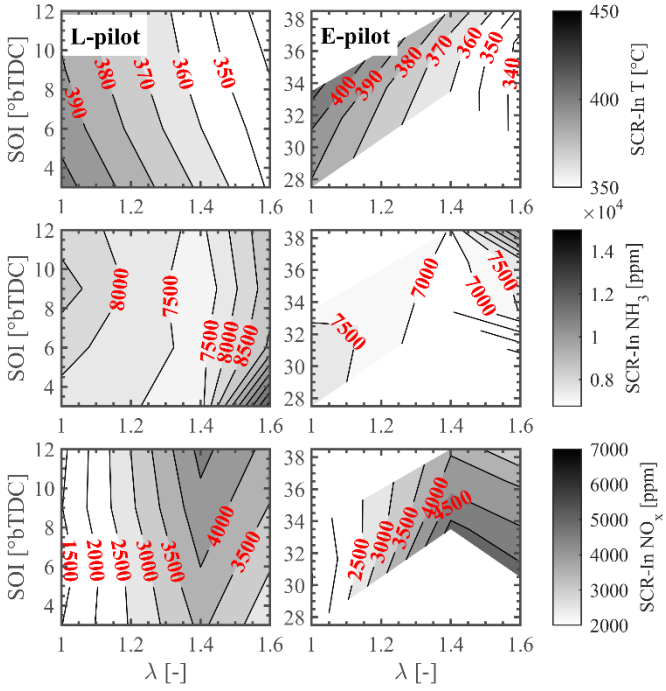

FIGURE 3: SCR-IN TEMPERATURE (TOP), NH_3 (MIDDLE) AND NO_x (BOTTOM) AS A FUNCTION OF DIESEL PILOT SOI AND λ. THE L-PILOT CASES ARE SHOWN ON THE LEFT, AND E-PILOT CASES ARE SHOWN ON THE RIGHT.

3. RESULTS AND DISCUSSION

3.1 SCR Inlet Conditions

3.1.1 NO_x, NH_3, and Exhaust Temperature

The inlet conditions generated for the SCR with both the L-pilot and E-pilot cases are shown in Figure 3 as a function of diesel pilot SOI and λ. First, it is evident that the sensitivity to λ is more pronounced for the temperature, NH_3, and NO_x (NO_2 < 30 ppm) at the SCR inlet. This is true regardless of the injection strategy being considered. The temperature ranges from about 340°C at a λ of 1.6 to about 400°C at a λ of 1.0 for both the L-pilot and E-pilot cases (ΔT between exhaust port and SCR-In varies from 50°C at λ of 1.6 to 100°C at λ of 1.0). The increase in temperature at a lower λ is driven by thermal efficiency in both instances. The unburned NH_3 generated from the in-cylinder combustion process exceeded the NO_x at any given λ value. In general, for both the L-pilot and E-pilot cases, a minimum in NH_3 was accompanied by a maximum in NO_x at a λ of 1.4. This inverse relationship suggests that the majority of the NO_x generated for these cases is fuel-borne and can be thought of as an incomplete combustion product of the premixed NH_3 [10]. At λ values less than 1.4, the inverse relationship falls apart, potentially indicating more complete conversion of the NH_3 that does burn. The E-pilot strategy generally also results in lower unburned NH_3 than that of the L-pilot, possibly influenced by the increased spatial availability of the high-reactivity fuel resulting in better consumption of the surrounding premixed NH_3 [10]. The space velocity, which affects the catalyst performance, does not change significantly as a function of λ: ~1.9E04 h^{-1} (SCR) and ~9.5E05 h^{-1} (ASC).

3.1.2 H_2O Concentration

The concentration of water in the exhaust is significantly higher for the dual-fuel cases than for conventional diesel-only operation (~9%), as shown in Figure 4. This is due to the high H content of the premixed fuel, which, when completely consumed, forms water in-cylinder. Such high concentrations of water in the exhaust can pose challenges for SCR, hindering NO_x conversion efficiency and increasing N_2O formation, especially at lower exhaust temperatures typical of low load operation [21, 22]. Under the exhaust temperature conditions evaluated in this study, the high-water effects on NO_x conversion performance may not play as important of a role.

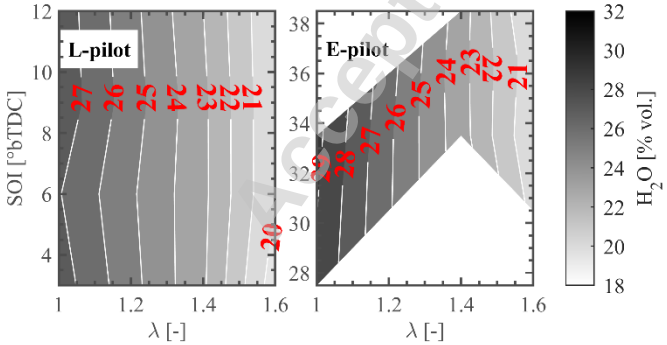

FIGURE 4: EXHAUST H_2O CONCENTRATION: L-PILOT (LEFT) AND E-PILOT (RIGHT).

3.1.3 Thermal Efficiency

Figure 5 shows the resulting thermal efficiency penalty for the dual-fuel cases relative to the baseline CDC case. For both the L-pilot and E-pilot cases, the thermal efficiency is similar to that of the CDC case at a λ of 1.4, but leaner or richer operation results in considerable penalty. Hence, optimal SCR performance at a λ of 1.4 would be desirable when considering factors such as thermal efficiency.

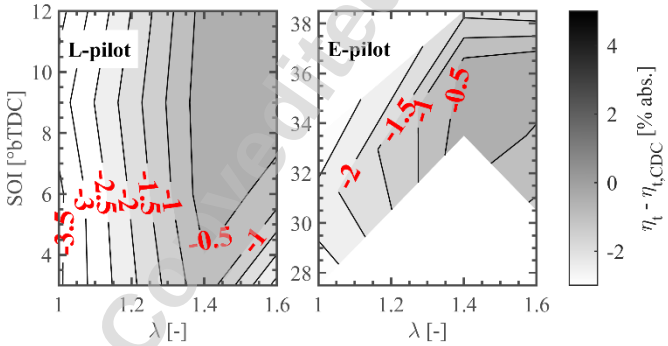

FIGURE 5: THERMAL EFFICIENCY PENALTY RELATIVE TO CDC BASELINE TO GENERATE THE INLET CONDITIONS FOR THE AFTERTREATMENT SETUP USING DUAL-FUEL NH_3 COMBUSTION: L-PILOT (LEFT) AND E-PILOT (RIGHT).

3.2 SCR Performance

3.2.1 NO_x Conversion

As shown in Figure 6, the NO_x conversion over the Cu-SCR exceeds 99% over the explored conditions for both the L-pilot and E-pilot strategies, despite greater than 20% water concentration in the exhaust (note the ANR exceeds a value of 1 under all conditions). Existing studies have explored the effect of water on Cu-SCR performance [23, 24, 25, 26]; however, to the best of the authors' knowledge, such high concentrations of water (due to greater than 90% substitution levels) have not been considered in the literature for a nontraditional fuel like ammonia. Work by Wan *et al.* [23], however, suggests that the presence of water can play a permanent positive role by allowing the migration of unanchored Cu ions to defect sites to form active sites for NO_x reduction. The presence of water at high temperatures can also decrease the reaction energy barrier of reoxidation of Cu^+ to Cu^{2+}, facilitating NO_x conversion over the Cu-SCR [25].

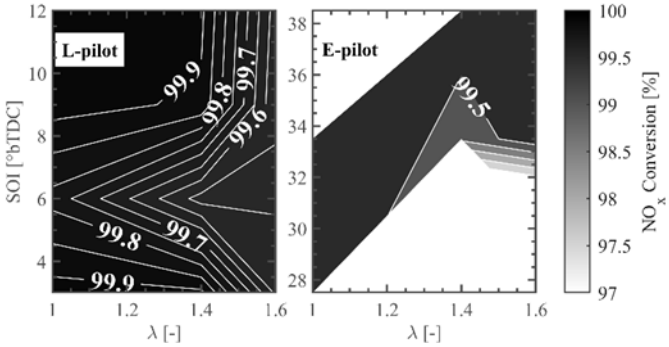

FIGURE 6: NO_x CONVERSION EFFICIENCY OF THE SCR SYSTEM: L-PILOT (LEFT) AND E-PILOT (RIGHT).

Owing to similar SCR inlet conditions, NO_x conversion, and SOI insensitivity for the L-pilot and E-pilot strategies, only the L-pilot results at a 12°bTDC SOI timing will be presented in the following sections for brevity.

The global reactions mainly responsible for NO_x reduction are as follows [27]:

$$4NO + 4NH_3 + O_2 \rightarrow 4N_2 + 6H_2O \text{ (Standard SCR)} \quad (1)$$
$$NO + NO_2 + 2NH_3 \rightarrow 2N_2 + 3H_2O \text{ (Fast SCR)} \quad (2)$$
$$2NO_2 + 4NH_3 + O_2 \rightarrow 3N_2 + 6H_2O \ (NO_2 - \text{SCR}) \quad (3)$$

It was noted earlier that the NO_2 concentrations are below 30 ppm across the explored space ($NO_x \approx NO$). This suggests that reaction (1) is the dominant mode for NO reduction over the SCR. The standard SCR reaction utilizes an equimolar concentration of NH_3 and NO_x (ANR = 1). Hence, a condition with ANR < 1 would result in insufficient NH_3 availability for complete NO conversion (NO slip), whereas ANR > 1 indicates excess NH_3 availability, potentially leading to NH_3 slip.
A sample set of NH_3, NO_x, and ANR values is shown in Figure 7 for the L-pilot strategy as a function of λ. The ANR approaches an ideal value of 1 as λ is decreased from 1.6 to 1.4, with a further decrease causing significant deviation from ideal stoichiometry. The deviation is caused by a reduction in fuel-borne NO because of high unburned NH_3. Note that the SCR-inlet temperature ranges from 334°C at λ of 1.6 to 387°C at λ of 1.0 for the cases shown in Figure 7. Within this temperature and space velocity range and at ANR > 1, high NO_x conversion was achieved, with NO_x concentrations not exceeding 10 ppm at the SCR outlet (Figure 6).

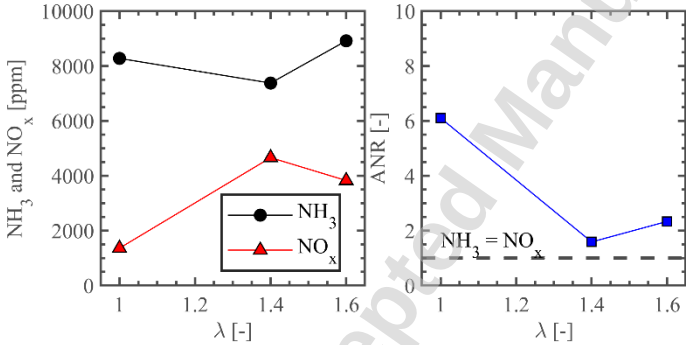

FIGURE 7: SCR-IN NH_3 AND NO_x VALUES (LEFT) AND ANR (RIGHT) AS A FUNCTION OF λ FOR THE L-PILOT CASE WITH SOI OF 12°BTDC.

3.2.2 NH_3 Slip and N_2O Penalty

As expected from the aforementioned discussion, the NH_3 slip results shown in Figure 8 (top) mirror the trend in ANR as a function of λ. However, the concentration of NH_3 required to satisfy a reaction (1) would result in a higher than observed NH_3 slip, as seen in Figure 8 (top). This can be attributed to the competitive, nonselective reactions of NH_3 with O_2, primarily occurring through reactions (4) and (5). The majority of the NH_3 consumption results from oxidation to N_2 at elevated temperatures [28, 29, 30, 31, 32]. The observed partial oxidation to N_2O is undesirable because it increases the CO_2-equivalent penalty.

$$2NH_3 + 2O_2 \rightarrow N_2O + 3H_2O \quad (4)$$
$$4NH_3 + 3O_2 \rightarrow 2N_2 + 6H_2O \quad (5)$$

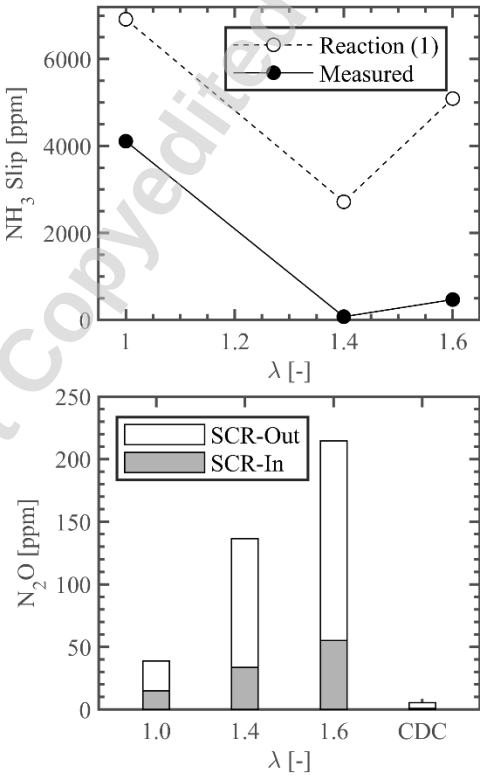

FIGURE 8: NH_3 SLIP THROUGH THE SCR (TOP) AND SCR-IN/SCR-OUT N_2O (BOTTOM) FOR THE L-PILOT CASE WITH SOI OF 12°BTDC. THE CDC SCR-IN/SCR-OUT N_2O RESULTS ARE SHOWN FOR REFERENCE IN THE BOTTOM PLOT.

These reactions may occur alongside the standard SCR reaction, consuming NH_3 without NO_x reduction, especially at higher temperatures (Figure 8 [bottom]) [28]. The selectivity to N_2O decreases at richer conditions as the concentration of O_2 available for reaction (4) is reduced. The SCR-Out N_2O emissions exceeded the CDC baseline value across all λ cases. Note that the CDC results were not generated by dosing the SCR with NH_3 and should be interpreted with caution (qualitative reference for the dual-fuel aftertreatment performance).

3.3 ASC Inlet Conditions

The inlet conditions generated for the ASC rely on the performance of the SCR placed upstream of it and differ considerably, as shown in Figure 9. Because O_2 measurements were unavailable at the ASC inlet, the concentrations were estimated based on reactions (1), (4), and (5), as shown:

$$[O_2]_{\text{ASC-In}} \approx [O_2]_{\text{SCR-In}} - [O_2]_{\text{Rxn (1)}} - [O_2]_{\text{Rxn (4)}} - [O_2]_{\text{Rxn (5)}}$$

$$[O_2]_{Rxn\,(1)} = \frac{[NO]_{SCR-In}}{4}$$

$$[O_2]_{Rxn\,(4)} = 2 \cdot ([N_2O]_{ASC-In} - [N_2O]_{SCR-In})$$

$$[O_2]_{Rxn\,(5)} = \frac{3 \cdot ([NH_3]_{SCR-In} - [NH_3]_{ASC-In} - [NH_3]_{Rxn\,(1)} - [NH_3]_{Rxn\,(4)})}{4}$$

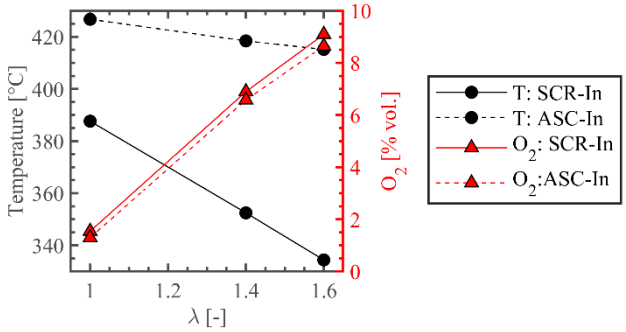

FIGURE 9: TEMPERATURE AND O_2 AVAILABILITY AT THE INLET OF THE SCR AND ASC AS A FUNCTION OF λ FOR THE L-PILOT CASE WITH SOI OF 12°BTDC. NOTE THAT THE SCR VALUES ARE SHOWN FOR REFERENCE, AND THE ASC-IN O_2 IS APPROXIMATED USING REACTIONS (1), (4) AND (5).

This approach assumes that (a) the entirety of the available NO at the SCR inlet participates in reaction (1); (b) reaction (4) is the dominant N_2O production pathway; and (c) the remainder of the NH_3 difference is accounted for via reaction (5). The exothermic nature of the SCR reactions results in $T_{ASC-In} > T_{SCR-In}$ across the tested λ conditions, as shown in Figure 9. The temperature exceeds a value of 400°C for every λ case, which is important for efficient ASC performance. However, the difference in O_2 concentration as a function of λ will play a more important role as the oxidation pathways rely on O_2 availability.

Following are the global reactions that may be relevant at these inlet conditions [33]:

$$4NH_3 + 3O_2 \rightarrow 2N_2 + 6H_2O \quad (6)$$
$$4NH_3 + 5O_2 \rightarrow 4NO + 6H_2O \quad (7)$$
$$2NH_3 + 2O_2 \rightarrow N_2O + 3H_2O \quad (8)$$

Reaction with N_2 in the products is the most thermodynamically favorable; however, undesired NO and N_2O can also be produced depending on reaction conditions and catalyst type.

3.4 ASC Performance

The ASC results shown in Figure 10 indicate high NH_3 conversion at leaner conditions, but a mere 30% at a λ of 1.0, resulting in 2,840 ppm of NH_3 at the ASC outlet. This is unsurprising, given the low O_2 concentration at λ=1. The leaner cases, on the other hand, result in less than 10 ppm of NH_3 at the outlet of the ASC owing to both O_2 abundance and lower initial NH_3 concentrations (<500 ppm). Figure 10 (bottom) also appears to show that reaction (8) is not a dominant pathway at the tested conditions because the change in N_2O across the ASC is negligible. Similar conclusions can be drawn for reaction (7) because the change in NO across the ASC was within the measurement uncertainty of the instruments used for the experiments (ASC-Out [NO] < 4 ppm). Under the conditions tested here, the ASC exhibited high selectivity for NH_3 oxidation to N_2, rather than to NO or N_2O.

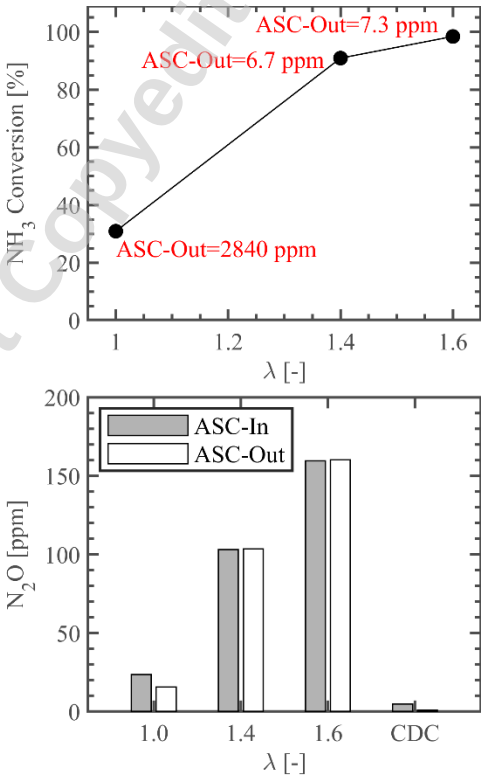

FIGURE 10: ASC NH_3 CONVERSION (TOP) AND ASC-IN/ASC-OUT N_2O (BOTTOM) AS A FUNCTION OF λ FOR THE L-PILOT CASE WITH SOI OF 12°BTDC. THE CDC ASC-IN/ASC-OUT N_2O RESULTS ARE SHOWN FOR REFERENCE IN THE BOTTOM PLOT.

The aftertreatment performance for the L-pilot cases is compared with that of the CDC baseline in terms of equivalent CO_2 emissions. These are calculated by considering the CO_2-equivalent impact of N_2O over a span of 100 years (273 × CO_2 [8]), as shown in Figure 11. Despite the formation of N_2O over the SCR, CO_2-equivalent emissions reductions are realized relative to CDC at the tested conditions. An approximately 44% reduction at a λ of 1.6 and an 88% reduction at a λ of 1.0 are evident. However, the 88% reduction is accompanied by a thermal efficiency penalty of ~3.5% (absolute) and high tailpipe NH_3 emissions (2,840 ppm). A λ of 1.4, however, provides a 60% reduction with similar thermal efficiency and less than 10 ppm tailpipe NH_3 emissions. More importantly, it is worth noting that these results were obtained under favorable exhaust temperature conditions. Lower temperatures (at lower loads) may result in

NO slip over the SCR or a CO_2-equivalent penalty relative to CDC due to N_2O selectivity. This is a part of the research scope and will be explored in the upcoming experimental efforts.

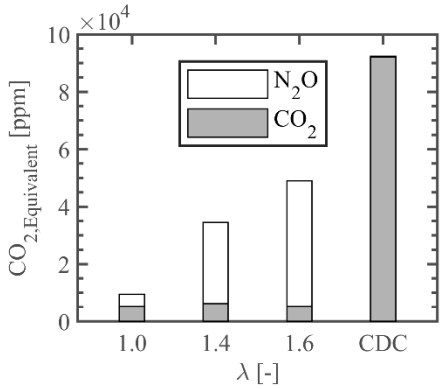

FIGURE 11: ASC-OUT CO_2-EQUIVALENT AS A FUNCTION OF λ FOR THE L-PILOT CASE WITH SOI OF 12°BTDC. THE CDC CO_2-EQUIVALENT RESULT IS SHOWN FOR REFERENCE.

Figure 12 provides a summary of the N-based emissions trends that were observed as a function of λ in this study.

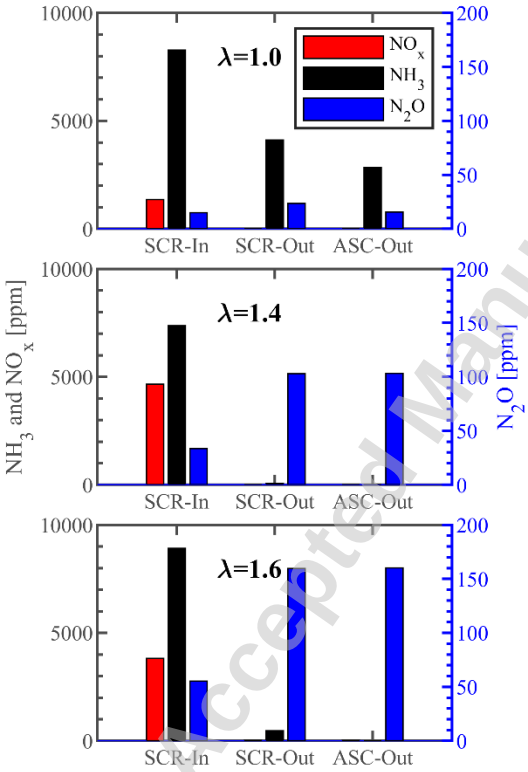

FIGURE 12: SUMMARY OF SCR-IN, SCR-OUT, AND ASC-OUT N-BASED EMISSIONS AS A FUNCTION OF λ FOR THE L-PILOT CASE WITH SOI OF 12°BTDC.

4. CONCLUSION

In this work, a medium-duty single-cylinder engine was used to evaluate the performance of a Cu-SCR and ASC system under dual-fuel diesel/NH_3 mode. The inlet conditions for the aftertreatment system were generated using two injection strategies, L-pilot and E-pilot, at engine speed and load of 1,200 rpm and 12.6 bar. The air flow commanded to the engine was varied to change the global λ with an NH_3 energy fraction of 95%. The SCR and ASC performance were evaluated at steady-state engine operation by sampling for N-based species using a FTIR at three locations: SCR-In, SCR-Out (ASC-In), and ASC-Out.

The following conclusions can be drawn from the results of this study:

- Both the L-pilot and E-pilot strategies generated similar temperatures, unburned NH_3, and NO_x emissions at the inlet of the SCR.
- The SCR was effective in converting NO_x, achieving over 99% conversion under the conditions studied.
- A λ of 1.4 provided an ANR of approximately 1.5, resulting in the lowest NH_3 slip over the SCR.
- NH_3 conversion over the ASC was the lowest at a λ of 1.0 despite an inlet temperature of 425°C due to limited O_2 availability under stoichiometric conditions.
- A 60% reduction in CO_2-equivalent relative to CDC was possible at a λ of 1.4 with similar thermal efficiency and less than 10 ppm tailpipe NH_3 emissions.

ACKNOWLEDGEMENTS

This research was supported by the Department of Energy's (DOE's) Vehicle Technologies Office (VTO) and the Department of Transportation's (DOT's) Maritime Administration (MARAD). We would like to thank Kevin Stork and Gurpreet Singh at the DOE VTO and Galen Hon and Will Nabach at the DOT MARAD for their guidance and support.

The authors would also like to thank Cummins for supplying the engine used for this study.

REFERENCES

[1] International Maritime Organization (IMO) , "Third IMO greenhouse gas study 2014," 2015.

[2] International Maritime Organization (IMO), "2023 IMO Strategy on Reduction of GHG Emissions from Ships (MEPC 80 Annex 15)," 2023.

[3] M. Aziz, A. T. Wijayanta, and A. B. D. Nandiyanto, "Ammonia as Effective Hydrogen Storage: A Review of Production, Storage and Utilization," *Energies,* 2020, doi:10.3390/en13123062.

[4] C. Li, T. Wang, and J. Gong, "Alternative Strategies Toward Sustainable Ammonia Synthesis," in *Transactions of Tianjin Univeristy, doi:10.1007/s12209-020-00243-x*, 2020.

[5] H. Kobayashi, A. Hayakawa, K. K. A. Somarathne, and E. C. Okafor, "Science and Technology of Ammonia Combustion," in *Proceedings of the Combustion Institute, doi: 10.1016/j.proci.2018.09.029*, 2018.

[6] Roney, Nickolette, and Fernando Llados, "Toxicology profile for ammonia," US Department of Health and Human Service , 2004.

[7] D.R. Lide, CRC Handbook of Chemistry and Physics, vol. 85, Boca Raton, FL, USA: CRC Press, doi:10.1201/b17118, 2004.

[8] B. Wu, Y. Wang, D. Wang, Y. Feng, and S. Jin, "[12] B. Wu, Y. Generation Mechanism and Emission Characteristics of N2O and NOx in Ammonia-Diesel Dual-Fuel Engine," *Energy,* 2023, doi: 10.1016/j.energy.2023.129291.

[9] S. Curran, B. Kaul and D. Tyrewala, "Mapping Ammonia-Diesel Combustion on a Single-Cylinder 107 mm Bore Diesel Engine Retrofitted for Ammonia Post-Fuel Injection," *IJER,* 2025.

[10] D. Tyrewala, B. Kaul, S. Curran and D. Splitter, "Experimental Investigation of Air-Fuel Equivalence Ratio Effects on Advanced Dual-Fuel Ammonia/Diesel Combustion on a Single-Cylinder Medium-Duty Diesel Engine at High Load," *Proceedings of the Combustion Institute ,* 2026.

[11] Nova I, Tronconi E, Fundamental and Applied Catalysis Urea-SCR Technology for deNOx after Treatment of Diesel Exhausts, Berlin, Germany: Springer, 2014, doi: 10.1007/978-1-4899-8071-7.

[12] Han J, Wang A, Isapour G, Harelind H, Skoglundh M, Creaser D, Olsson L., "N2O formation during NH3-SCR over different zeolite frameworks: effect of framework structure, copper species, and water," *Industrial & Engineering Chemistry Research,* vol. 60, no. 49, 2021, doi: 10.1021/acs.iecr.1c02732.

[13] Wang A, Wang Y, Walter ED, Kukkadapu RK, Guo Y, Lu G, Weber RS, Wang Y, Peden CH, Gao F., "Catalytic N2O decomposition and reduction by NH3 over Fe/Beta and Fe/SSZ-13 catalysts.," *Journal of Catalysis ,* vol. 358, pp. 199-210, 2018, doi: 10.1016/j.jcat.2017.12.011.

[14] Voniati, G, Dimaratos A., Koltsakis G., Ntziachristos L., "Emission Control Concepts for large two-stroke ammonia engines," in *Proceedings of the 8th Rostock Large Engine Symposium* , 2024.

[15] Oh, S., Park, C., Ahn, M., Jang, H., & Kim, S., "Experimental approach for reducing nitrogen oxides emissions from ammonia–natural gas dual-fuel spark-ignition engine," *Fuel ,* vol. 332, no. 2, 2023, doi:10.1016/j.fuel.2022.126065.

[16] Kuta, K., Przybyła, G., Kurzydym, D., & Żmudka, Z., "Experimental and numerical investigation of dual-fuel CI ammonia engine emissions and after-treatment with V2O5/SiO2–TiO2 SCR," *Fuel,* vol. 334, no. 2, 2023, doi:10.1016/j.fuel.2022.126523.

[17] Liu G, Zhang H, Li Y, Wang P, Zhan S., "Selective catalytic reduction of NO x with NH 3 over copper-based catalysts: recent advances and future prospects," *EES Catalysis,* vol. 2, 2024, doi:10.1039/D3EY00210A.

[18] Xiang P, Liu J, Zhao W, Ji Q, Ao C, Wang X, Sun P, Wang X, Li Z., "Experimental investigation on gas emission characteristics of ammonia/diesel dual-fuel engine equipped with DOC+ SCR aftertreatment," *Fuel,* vol. 359, 2024, doi:10.1016/j.fuel.2023.130496.

[19] Sun X, Li M, Li J, Duan X, Wang C, Luo W, Liu H, Liu J., "Nitrogen oxides and ammonia removal analysis based on three-dimensional ammonia-diesel dual fuel engine coupled with one-dimensional SCR model.," *Energies,* vol. 16(2), 2023, doi:10.3390/en16020908.

[20] S. Curran, J. Szybist, B. Kaul, J. Easter, and S. Sluder, "Fuel Stratification Effects on Gasoline Compression Ignition with a Regular-Grade Gasoline on a Single-Cylinder Medium-Duty Diesel Engine at Low Load," in *SAE Technical Paper 2021-01-1173*, 2021, doi: 10.4271/2021-01-1173.

[21] Deka, D.J., Lee, G., Rappé, K.G., Walter, E., Szanyi, J. and Wang, Y.,, "Influence of H 2-ICE specific exhaust conditions on the activity and stability of Cu-SSZ-13 deNO x catalysts," *Catalysis Science & Technology,* 2025.

[22] Wang X, Chi R, Gu L, Sun L, Liu Y, Wu Z., "Effect of water vapor on low temperature SCR performances over Cu and Mn-based catalysts: A comparison study.," *Journal of Rare Earths,* 2024, doi: 10.1016/j.jre.2024.06.038.

[23] Wan Y, Yang G, Xiang J, Shen X, Yang D, Chen Y, Rac V, Rakic V, Du X., "Promoting effects of water on the NH 3-SCR reaction over Cu-SAPO-34 catalysts: transient and permanent influences on Cu species," *Dalton Transactions ,* no. 3, 2020, doi: 10.1039/C9DT03848E.

[24] Gao F, Mei D, Wang Y, Szanyi J, Peden CH., "Selective catalytic reduction over Cu/SSZ-13: linking homo-and heterogeneous catalysis," *Journal of the American Chemical Society,* vol. 139, no. 13, 2017, doi: 10.1021/jacs.7b01128.

[25] Shi L, Zhang J, Shen G, Fan D, Wen Y, Zhao Y, Chen R, Shen M, Shan B., "Water mediated oxygen activation in NH 3 SCR reaction over a Cu-SAPO-34 catalyst: a first principles study," *Catalysis Science & Technology,* no. 5, 2019, doi: 10.1039/C8CY02618A.

[26] Liu Y, Xue W, Seo S, Tan X, Mei D, Liu CJ, Nam IS, Hong SB., "Water: A promoter of ammonia selective catalytic reduction over copper-exchanged LTA zeolites.," *Applied Catalysis B: Environmental,* vol. 294, 2021, doi: 10.1016/j.apcatb.2021.120244.

[27] Gui R, Yan Q, Xue T, Gao Y, Li Y, Zhu T, Wang Q., "The promoting/inhibiting effect of water vapor on the selective catalytic reduction of NOx," *Journal of Hazardous Materials ,* vol. 439, 2022, doi: 10.1016/j.jhazmat.2022.129665.

[28] Zhu M, Lai JK, Wachs IE, "Formation of N2O greenhouse gas during SCR of NO with NH3 by supported vanadium oxide catalysts," *Applied Catalysis B: Environmental,* vol. 224, pp. 836-840, 2018, doi: 10.1016/j.apcatb.2017.11.029.

[29] Martín JA, Yates M, Ávila P, Suárez S, Blanco J., "Nitrous oxide formation in low temperature selective catalytic reduction of nitrogen oxides with V2O5/TiO2 catalysts," *Applied Catalysis B: Environmental,* vol. 70, no. 1-4, pp. 330-334, 2007, doi: 10.1016/j.apcatb.2005.11.026.

[30] Chen S, Vasiliades MA, Yan Q, Yang G, Du X, Zhang C, Li Y, Zhu T, Wang Q, Efstathiou AM, "Remarkable N2-selectivity enhancement of practical NH3-SCR over Co0. 5Mn1Fe0. 25Al0. 75Ox-LDO: The role of Co investigated by transient kinetic and DFT mechanistic studies," *Applied Catalysis B: Environmental,* vol. 277, 2020, doi: 10.1016/j.apcatb.2020.119186.

[31] Metkar PS, Harold MP, Balakotaiah V, "Experimental and kinetic modeling study of NH3-SCR of NOx on Fe-ZSM-5, Cu-chabazite and combined Fe-and Cu-zeolite monolithic catalysts," *Chemical Engineering Science,* vol. 87, pp. 51-66, 2013, doi: 10.1016/j.ces.2012.09.008.

[32] Nedyalkova R, Kamasamudram K, Currier NW, Li J, Yezerets A, Olsson L, "Experimental evidence of the mechanism behind NH3 overconsumption during SCR over Fe-zeolites," *Journal of Catalysis,* vol. 299, pp. 101-108, 2013, doi: 10.1016/j.jcat.2012.11.009.

[33] Gil ES., "Evaluation of Ammonia Slip Catalysts, Master's Thesis," CHALMERS UNIVERSITY OF TECHNOLOGY, Goteborg, Sweden, 2013.

LIST OF TABLES

LIST OF FIGURES